Characterizing auroral absorption based on geomagnetic hourly range

R. A. D. Fiori[1], L. Trichtchenko[1], C. Balch[2], E. Spanswick[3], S. Groleau[1]

[1]Geomagnetic Laboratory, Natural Resources Canada, Ottawa, Ontario, Canada

[2]NOAA Space Weather Prediction Center, Boulder, Colorado, USA

[3]Department of Physics and Astronomy, University of Calgary, Calgary, Alberta, Canada

Contact: Robyn Fiori

robyn.fiori@canada.ca

613-837-5137 (office)

613-882-3904 (temporary)

Key points: space weather, ionospheric absorption**,** auroral absorption, geomagnetic field

Abstract

Energetic electron precipitation is a source of both ionospheric and geomagnetic disturbances. The resultant increased ionization in the auroral oval leads to the absorption of high frequency radio waves in the auroral zone, or auroral absorption. Auroral absorption is typically characterized by global geomagnetic activity indices, such as the Kp index. In this paper the hourly range of the magnetic field (HR) is examined as an alternative to the 3-hour Kp index for describing the dynamic and localized features of auroral absorption represented by the hourly range of absorption (HRA). Kp, magnetometer, and riometer data were examined for a 3-year period for stations spread across typical auroral latitudes. A general linear relationship was shown to exist between Kp and LOG_{10}(HRA) for Kp<4; for Kp≥4 the correlation was weaker. A stronger linear correlation was demonstrated between LOG_{10}(HRA) and LOG_{10}(HR) for HR >50 nT, characterized by a correlation coefficient of R=0.63. Increased variability in the relationship between HRA and Kp was attributed to the following factors: the variability of the magnetic field within the 3-hour window characterized by the Kp-index which was better represented by a 1-hour HR; the dependence of the Kp index on sub-auroral magnetic data which is not subject to the energetic electron precipitation experienced within the auroral region; and reduced statistics for Kp>6.

1. Introduction

Energetic electron precipitation due to magnetospheric-ionospheric coupling, occurring both on a regular basis, and intensified through space weather contributions originating from the sun, leads to enhanced ionization in the ionosphere at auroral latitudes causing both ionospheric and geomagnetic disturbances [e.g., Baker et al., 1981; Hargreaves, 1969; Liang et al., 2007; Newell et al., 2001].

At D-region altitudes (75-95 km), the precipitation of high energy (>30 keV) magnetospheric electrons causes a phenomenon known as auroral absorption which impacts the transmission of high frequency (HF) (3-30 MHz) radiowave signals. Impacted systems include over-the-horizon-radar (OTHR) used for long-range surveillance (Thayaparan el al., 2018) and research (e.g., Chisham et al., 2007), and HF communications systems used, for example, by the military, aviation, emergency management, coast guard, and marine transport (e.g., Agy, 1970; Cannon et al., 2013; Coyne, 1979; National Research Council, 2008; Neal et al., 2013; Pirjola et al., 2005). Recognizing the need for an operational advisory service to mitigate the impacts of ionospheric disturbances to aviation, the International Civil Aviation Organization (ICAO) initiated the development of such a service, which began operation on 08 November 2019. ICAO specifically identifies auroral absorption as a threat to international aviation (ICAO, 2018; 2019).

In general, absorption is a reduction of the signal strength of a transmitted radiowave caused by interactions with ionospheric particles. Absorption is most commonly observed in the D-region due to the relatively high concentration of neutral particles and, in particular, is dependent on particle collision frequency and recombination rates. Absorption is enhanced when electron density is increased due to increased ionization. There are 3 primary sources of D-region absorption; each is attributed to a different ionization source: (1) Shortwave fadeout (SWF) is a short-lived (typically <2 hours) dayside phenomenon caused by photoionization by radiation emitted during solar X-ray flares (e.g., Frissell et al., 2014). (2) Polar cap absorption (PCA) is caused by the precipitation of energetic solar protons, usually associated with a coronal mass ejection. PCA events can be long-lived (~days), impacting the high-latitude region and reaching as far equatorward as ~60-65° magnetic latitude with primary impacts on the dayside. (e.g., Hargreaves, 2010; Kavanagh et al., 2004). (3) Auroral absorption caused by the energetic electron precipitation at auroral latitudes. This paper focuses on auroral absorption.

Auroral absorption is a highly structured (spatially and temporally) phenomenon with an occurrence and magnitude that varies in magnetic latitude (MLAT) and magnetic local time (MLT). Auroral absorption typically peaks between 64° and 68° MLAT in both the pre-noon (MLT) and midnight sectors (Basler, 1963; Driatsky, 1966; Frank-Kamenetsky and Troshichev, 2012; Hargreaves 1969; Hartz et al., 1963; Hook, 1968). Substorm activity and related electron precipitation cause the midnight peak (Hargreaves, 2010; Kavanagh et al., 2004) whereas the pre-noon peak is caused by the eastward drift of substorm injected electrons in association with keV-energy diffuse auroral electrons (Kavanagh et al., 2004; Yamagishi et al., 1998). Auroral absorption events (> 0.5 dB) last on the order of 1-3 hours (Hargreaves, 2010), and are sporadic and irregular in behaviour (Kavanagh et al., 2004). Due to seasonal variation of magnetospheric geometry, absorption events are more frequent and 1.5-2 times stronger in winter months than summer months (Hargreaves, 1969; Newell et al., 2001; Yamagishi et al., 1998).

Given the impacts of radiowave absorption and reliance on affected infrastructure, it is highly desirable to develop absorption models to accurately describe absorption levels and impacted frequencies. Modelling requires an understanding of the different kinds of D-region absorption, which are driven by

different space weather phenomenon and have different characteristics. Absorption models do exist for modelling SWF and PCA (e.g., Sauer and Wilkinson, 2008; Rogers and Honary, 2015; Rogers et al. 2016; Fiori and Danskin, 2016). One example includes the D Region Absorption Prediction (D-RAP) model, which is operated by the Space Weather Prediction Center (SWPC) of the National Oceanic and Atmospheric Administration (NOAA) (http://wwwswpc.noaa.gov/products/d-region-absorption-predictions-d-rap).

Although an established and widely accepted operational model for auroral absorption has not been incorporated into tools like D-RAP, considerable work has gone into the development of both statistical models and statistical prediction models to characterize auroral absorption parameterized using the Kp or Ap index (e.g. Foppiano and Bradley, 1983, 1984; Hartz, 1963; Hartz et al. 1963; Hargreaves, 1966; 2007; Hargreaves and Cowley, 1967; Hargreaves et al., 1987; Holt et al., 1961; Kavanagh et al., 2004; Rogers et al. 2016).

A correlation between ionospheric and ground-based magnetic data during auroral absorption is not surprising, as both are directly related to the dynamics of electrons during magnetospheric disturbances, as discussed in Hargreaves (1969) and Liang et al. (2007). Additional studies examine the relationship between auroral absorption and magnetic parameters such as the polar cap (PC) index (Frank-Kamenetsky and Troshichev, 2012), solar wind parameters (Kavanagh et al., 2004; Ogunmodimu, 2016), and substorm-related phenomenon (e.g., Baker et al., 1981; Spanswick et al., 2005). Frank-Kamenetsky and Troshichev (2012) demonstrate the advantage of magnetic indices over magnetic field time series for comparing magnetic and ionospheric data. By reducing variations in the ionospheric data over 1 hour to the 1-hour maximum they were able to draw comparisons between the polar cap (PC) index and auroral absorption. Frank-Kamenetsky and Troshichev (2012) argue that the use of a 1-hour maximum accounts for any existing delays between the mechanisms leading to enhancements in the PC index and particle precipitation into the auroral region.

In this paper we focus on parameterization of auroral absorption derived from riometer observations by ground-based magnetic data (both global and local indices). One aspect of this paper is to investigate the accuracy of using the Kp index to describe auroral absorption. Kp is a global index whereas auroral absorption has been shown to be a more localized phenomenon with characteristic enhancements in the pre-noon and midnight sectors at auroral latitudes. Also, as Kavanagh et al. (2004) point out, Kp is a 3-hour index incapable of capturing the dynamic nature of auroral absorption. Finally, Kp represents the variation of the geomagnetic field at sub-auroral latitudes, where its contributing stations are located. However, at auroral latitudes, geomagnetic activity is largely driven by the precipitation of energetic electrons which is not necessarily the dominant signal at sub-auroral stations.

Another aspect of this paper is to examine the relationship between the global Kp index and the magnetic field hourly range at individual observatories with absorption observed locally at auroral latitudes. Localization of the magnetic field variations that go into the Kp index can be achieved by examining the underlying measurements, specifically the range of the magnetic field at individual observatories. In particular, we consider the range of the horizontal component of the magnetic field determined over one hour and make comparisons to the range of the absorption observed over the same interval for collocated stations. Such an approach will potentially remove the limitations of a global 3-hour sub-auroral index to characterize a more local and dynamic auroral phenomenon.

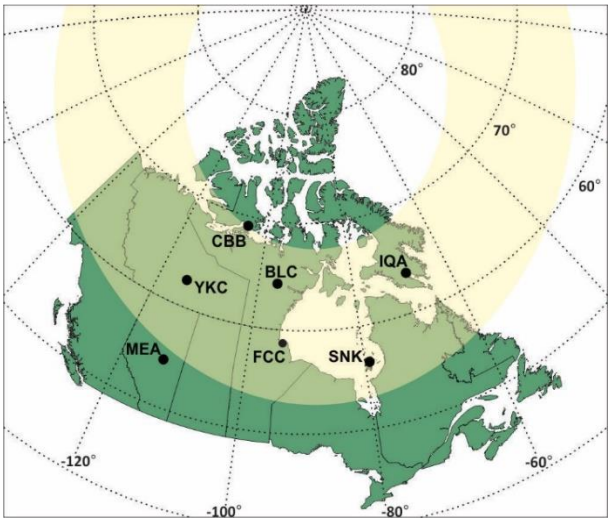

Figure 1: Geographic location of co-located riometer and magnetometer instruments. Yellow shading indicates the approximate location of the auroral oval, bounded by 63° and 77° magnetic latitude.

This paper is organised as follows: Section 2 describes the instrumentation and data used in the analysis, Section 3 presents the results of the study, which is followed by the discussion in Section 4, and conclusions and further recommendations in Section 5.

2. Data and Instrumentation

Canada provides an ideal landscape for auroral absorption studies due to the significant number of co-located riometer and magnetometer sites with instruments distributed across a wide band of latitudes spanning polar cap, auroral, and sub-auroral regions.

In an attempt to quantify the general relationship between absorption and geomagnetic data, one hour variations in both data sets are considered by comparing the hourly range of the absorption (HRA) data, determined by subtracting the maximum and minimum absorption in a one-hour period, to both the Kp (general 3-hour index) and HR (local 1-hour index), as described below.

Figure 1 shows the location of the 7 Canadian stations with co-located riometer and magnetometer instruments. The riometer station located at Fort Churchill (FCC) is operated by the University of Calgary (U of C) as a part of the Geospace Observatory Riometer Network (GO-RIO) (Rostoker et al., 1995). Riometer stations located at Cambridge Bay (CBB), Yellowknife (YKC), Baker Lake (BLC), Iqaluit (IQA), Meanook (MEA), and Sanikiluaq (SNK) are operated by the Natural Resources Canada (NRCan) network (Danskin et al., 2008; Lam, 2011). All geomagnetic observatories are operated by NRCan. Note the high concentration of stations within the typical location of the auroral oval (yellow shading). All data available for the BLC, CBB, IQA, MEA, SNK, and YKC for 2015-2017 were considered. Additionally the FCC magnetometer (NRCan) and riometer (U of C) data were considered for the 2001-2003 (prior to the installation of the NRCan riometers) to increase the data set in an attempt to incorporate periods of higher geomagnetic activity. The FCC data were not considered during the 2015-2017 period due to excessive noise contamination of the riometer component of the data. Table 1 lists the station coordinates and the data collection period considered for this study

Table 1: Station name, station name abbreviation, geographic coordinates of co-located riometer stations and geomagnetic observatories, and data collection period considered in this study.

Station	Abbreviation	Geographic Latitude	Geographic Longitude	Data collection
Baker Lake	BLC	64.3°	264.0°	2015-2017
Cambridge Bay	CBB	69.1°	255.0°	2015-2017
Fort Churchill	FCC	58.8°	265.9°	2001-2003
Iqaluit	IQA	63.7°	291.5°	2015-2017
Meanook	MEA	54.6°	246.7°	2015-2017
Sanikiluaq	SNK	56.5°	280.8°	2015-2017
Yellowknife	YKC	62.5°	245.5°	2015-2017

2.1 Absorption data

Absorption is quantified using the opacity of the ionosphere to cosmic radio noise from extra-terrestrial sources as measured by a relative ionospheric opacity meter, also known as a riometer. Riometers measure a signal in volts. Deviation of the measured voltage from a quiet-day value or quiet day curve (NORSTAR, 2014), expressed in dB, gives absorption. During quiet periods absorption is near zero at 30 MHz, which is the operating frequency of riometers used in this study, but peaks of up to 6 dB have been observed with auroral absorption (Nielsen and Honary, 2000).

Riometers considered in this study have a dual-dipole broad-beam (wide beam) antenna operating at 30 MHz and detect absorption over an area spanning a ~100 km diameter within the ionosphere over the riometer. Data are provided at a 1-s resolution. Due to the relative manner in which absorption is determined (i.e., deviation from a quiet day curve value), low absorption values of <0.2 dB are discarded from this study (e.g., Foppiano and Bradley, 1984).

Riometer data were filtered to remove noise contamination, environmental noise, and instrument failure. Noise contamination in the riometer data was removed by filtering the data set for periods where the absorption was consistently <0.2 dB or the HRA was <0.1dB.

2.2 Geomagnetic data

Magnetic data used in this study was obtained from the NRCan Canadian Magnetic Observatory System (CANMOS) (https://geomag.nrcan.gc.ca/obs/canmos-en.php). CANMOS is composed of 14 magnetic observatories distributed throughout Canada operating fluxgate magnetometers (Serson, 1957) to observe variations in the intensity of the Earth's magnetic field, and a proton magnetometer. Data are reported in 3 orthogonal components (X, Y, Z) in a geodetic coordinate system representing the north (B_x), east (B_y), and radially inward (B_z) magnetic field components. Data from the fluxgate magnetometer are sampled at a frequency of 8 Hz, despiked, and resampled to 1 Hz using a 9-point rectangular filter. The 1 Hz data are filtered again using a 49 point Gaussian filter and resampled to a 5-second resolution to match the frequency of the proton magnetometer data. The 5-second data are filtered one more time using a 19 point Gaussian filter and resampled at a 1-minute interval. The 1-minute data are used in this study.

The Canadian Space Weather Forecast Center uses an additional magnetic parameter called the magnetic field hourly range to characterize magnetic activity (Hruska and Coles, 1987; Trichtchenko et al., 2009). Hourly range (HR) is determined in the X and Y directions by calculating the difference

between the maximum and minimum magnetic field data based on 1-minute magnetic field values over a period of 1 hour. HR values used in this study are the maximum HR determined from the X and Y components to represent the maximum magnetic field deviation observed. By definition HR is a positive value, removes the effects of long term secular variation, and minimizes the effects of slowly varying current systems such as the solar quiet (Sq) current system (which is relatively weak at high latitudes). HR smooths rapid-scale variations in the magnetic field while maintaining large-amplitude wave structures to provide an overall characterization of magnetic field activity.

2.3 Kp Index

The Kp index characterizes global magnetic activity based on the magnetic perturbation at 13 different magnetic observatories distributed across the globe at primarily sub-auroral latitudes (e.g., https://www.gfz-potsdam.de/en/kp-index/; Menvielle and Berthelier, 1991). For each station the maximum fluctuation of the magnetic disturbance (i.e. the range of the magnetic field component) is measured for the two horizontal magnetic field components, after subtracting Sq variations, in eight 3-hour intervals. The more disturbed component is converted to a quasi-logarithmic scale ranging from 0 to 9 using a data table specific to each location to determine the local K-index for each station. The scaling is done so that the station K-index frequency distributions from all observatories are approximately the same. The K-index is a local index specifically indicative of activity at the location of the observatory. Conversion tables are used to convert the K-index to the standardized Ks index, which also varies from 0 to 9, but is broken into thirds. For example, Kp=3-, 3o, and 3+ corresponds to 3-1/3, 3, and 3+1/3, respectively. Standardization eliminates seasonal and local time effects. The Kp index is determined as the average value of the Ks index values for the 13 stations. Kp < 3 corresponds to quiet conditions, Kp 5-6 represents moderate to strong conditions, and Kp>8 is considered severe to extreme. All Kp data used in this study were obtained from the National Geophysical Data Centre (NGDC) (ftp://ftp.ngdc.noaa.gov/STP/GEOMAGNETIC_DATA/INDICES/KP_AP/).

2.4 Data filtering

The data set was filtered to evaluate auroral absorption by removing periods contaminated by PCA and SWF. PCA event periods were identified using the solar proton event (SPE) list maintained by the NOAA Space Weather Prediction Center (SWPC) located at ftp://ftp.swpc.noaa.gov/pub/indices/SPE.txt. For each event in the SPE list, data corresponding to times between the SPE start time (rounded back to the nearest hour) and the SPE end time (rounded ahead to the nearest hour) were removed. In the 2015-2017 time period there were only 4 SPE events in the list. An additional PCA event, apparently missing from the SPE list, was included for filtering: 10 September 2017 17:00 UT to 13 September 2017 20:00 UT. This was a relatively significant event with a >10 MeV solar proton flux peaking at 1071.8 pfu with observable impacts to HF radiowave propagation (Frissell et al., 2019; Redmon et al., 2018). The 2001-2003 period was a much more active time in the solar cycle and data corresponding to 50 events were removed.

Data on solar X-ray flares were obtained from the NOAA NGDC in the form of GOES XRS reports which are available by year from 1975 onward (https://www.ngdc.noaa.gov/stp/space-weather/solar-data/solar-features/solar-flares/x-rays/goes/xrs/). All periods potentially contaminated by SWF due to 'M' and 'X' class flares were removed. For each solar X-ray flare data between the flare start time (rounded back to the nearest hour) and the flare end time (rounded ahead to the nearest hour) were

removed. For the joint 2001-2003 and 2015-2017 periods, data corresponding to 742 and 142 M and X-class solar X-ray flares were removed, respectively.

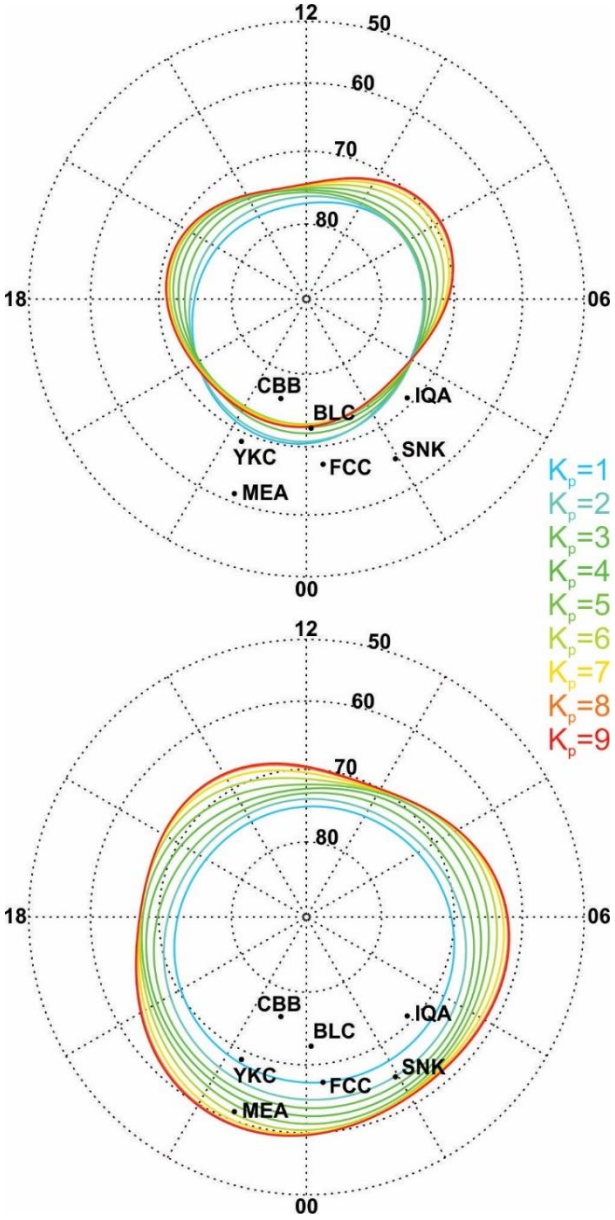

Figure 2: (Upper) Poleward and (lower) equatorward edge of the auroral oval modelled using the Starkov (1994) auroral boundary model as summarized in Sigernes et al. (2011). Boundaries are plotted for Kp=[1,9] in magnetic latitude / MLT coordinates. Possible location of the co-located riometers and magnetometers used in this study are overplotted.

Additional filtering was performed to ensure data were limited to the auroral region where auroral absorption is expected to be observed. The auroral zone was modelled using the Starkov (1994) auroral boundary model as summarized in Sigernes et al. (2011). The Starkov (1994) model provides the poleward and equatorward boundary of the auroral oval (used in this study) as well as the equatorward boundary of the diffuse aurora (not used in this study). The magnetic latitude and MLT for each data point was evaluated against the auroral oval boundaries calculated for the observed Kp value to eliminate points expected to be outside of the auroral oval.

Figure 2 shows the poleward and equatorward boundaries of the Starkov (1994) auroral oval for Kp=1,2,3…,9. As the geomagnetic activity level increases both boundaries expand to more equatorward latitudes. Overplotted are possible locations of the riometers considered in this study for a period when the Canadian sector is centered over the nightside. The CBB station is generally poleward of the auroral region, with the exception of a brief period near 12 MLT for Kp≤2. The BLC station straddles the poleward boundary of the auroral oval, drifting in and out of the auroral zone depending on geomagnetic activity level and MLT. The IQA and FCC stations are almost entirely located within the auroral zone. In the orientation illustrated in Figure 3, the SNK and MEA stations are located within the auroral zone for Kp≥2 and ≥5, respectively, but briefly shift equatorward of the auroral zone on the dayside into the evening sectors. The auroral location of the MEA station is interesting when considering that MEA is one of the 13 stations contributing to the Kp index, a point also made by Menvielle and Berthelier (1991).

3. Results

Analysis of the correlation between magnetometer and riometer observations begins with the qualitative examination of specific fluctuations for a single event. The comparison is generalized to consider larger-scale fluctuations through comparison of magnetometer-derived products such as the Kp index and the magnetic field hourly range.

Riometers respond to changes in the ionospheric electron density due to increased ionization, whereas magnetometers respond to local magnetic disturbances that result from electric currents flowing through the regions of enhanced ionization. A one-to-one relationship between absorption and magnetic data is not expected. Riometers used in these studies have a limited field of view centered above the riometer location with a focus on D-region phenomenon whereas the magnetometers react to auroral electrojet currents flowing at a slightly higher altitude of ~100 km influenced by ionospheric and magnetospheric processes also acting outside of the riometer field of view. For this reason a correlative rather than exact relationship between absorption and magnetic field is typically investigated through magnetic indices in contrast to direct comparisons with the magnetic field time series.

3.1 Event study: 07 January 2015

As an example, consider Figure 3 which illustrates variations in the X (north) and Y (east) components of the magnetic field observed at Baker Lake on 07 January 2015. The lower panel shows the absorption observed by the collocated BLC riometer. Large perturbations in the H component of the magnetic field on the nightside shortly after 9 UT correspond to large perturbations in the absorption. Both instruments observe activity having a quick onset lasting roughly 1.5 hours, but the riometer and magnetometer traces don't match exactly. This example illustrates that a general relationship is observed between absorption and magnetic data; there is no one-to-one correspondence between the minute-by-minute small-scale fluctuations in the data.

3.2 Distribution of Kp, HR, and HRA

Figure 4 shows histograms of Kp index, LOG_{10}(HR), and LOG_{10}(HRA) and probability distribution functions (PDFs) of Kp, HR, and HRA for the data set under consideration. Black bars and black filled circles are for the overall data set, prior to filtering out PCA and SWF events, for all magnetic latitudes and MLT's, and blue filled circles in the lower plots indicate the PDF for the filtered data set. Data with HRA<0.1 dB

in Figure 4c and Figure 4f have been removed to avoid noise contamination. Note that since Kp is already quasi-logarithmic by definition, the x-axis for the Kp histogram and the Kp PDF is not logarithmic.

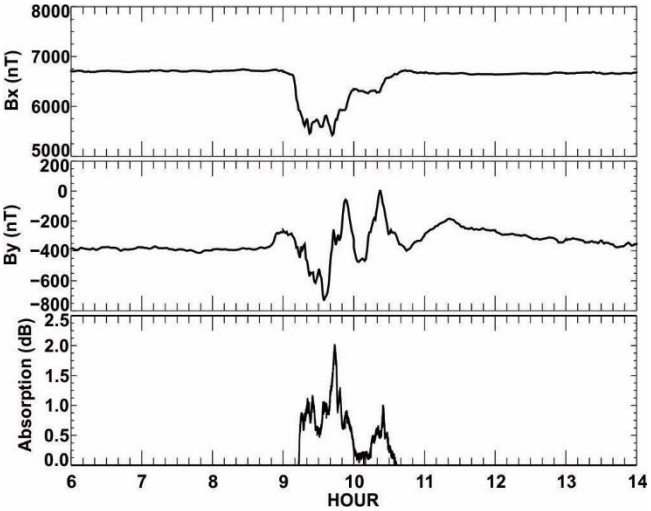

Figure 3: B_x (north) and B_y (east) components of the geomagnetic field and absorption observed by collocated magnetometer and riometer instruments at BLC on 07 January 2015. BLC riometer data have been filtered to remove noise.

Red curves in the upper plots represent the best-fit normal distribution.

Figure 4a and d show the Kp distributions. The histogram plot for the overall data set is consistent with a log-normal (Kp is quasi-logarithmic) distribution peaking at Kp=1o and falling off rapidly as activity level increases. Observation of a log-normal distribution is consistent with Mayaud (1976) who demonstrated a log-normal distribution in the K-index for two sub-auroral stations. Based on the PDF in Figure 4d, there is a minor separation between the filtered and unfiltered data sets; there is a slight reduction in low Kp<2 data and high Kp>7, and an increase in the distribution for Kp=[2,7].

The shift in the distribution for the filtered and unfiltered data sets can be explained through an understanding of the phenomenon and Kp. Filtering based on auroral oval location reduces the data set to 30% of its original size. Given the shape of the auroral oval, illustrated in Figure 3, the reduced data predominately corresponds to the nightside where geomagnetic activity level is expected to be enhanced. The only exception is for the CBB station which, due to its high latitude location, is only located within the auroral oval on the dayside between 10 and 15 MLT. The overall rise in the occurrence of Kp=[2,7] is not surprising. Why this effect does not expand to Kp>7 can be explained by the removal of PCA events.

If filtering is limited to the removal of PCA and SWF data only, and filtering by location with respect to the auroral oval boundary is ignored, then the distributions completely overlap for Kp ≤ 6, and the filtered distribution is slightly lower than the overall distribution for Kp > 6. This shift is expected as longer duration expulsions of solar energetic particles that cause PCA are often associated with a CME which can cause strong geomagnetic activity, and therefore high Kp, once it reaches the Earth (e.g., Desai and Giacalone, 2016). Removing periods of PCA removes these intervals.

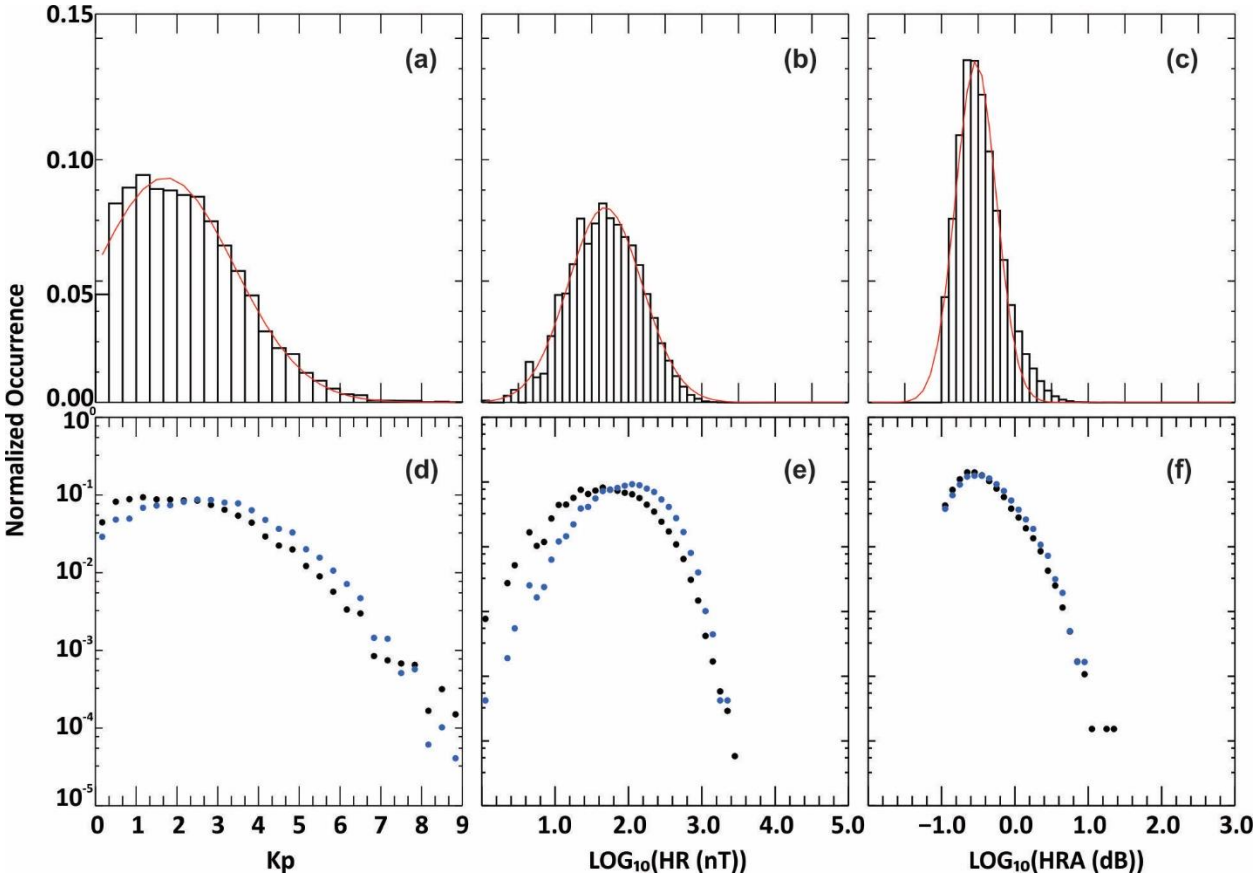

Figure 4: Distribution of (a) Kp, (b) LOG_{10} (HR), and (c) LOG_{10} (HRA) for all available data for the BLC, CBB, IQA, MEA, SNK, and YKC for 2015-2017, and FCC for 2001-2003. Red curves indicate the best-fit normal distribution to data. In (d), (e), and (f) the distributions are plotted with a logarithmic occurrence. Black filled circles indicate the original distributions from (a), (b), and (c), and blue filled circles are for the distribution of the filtered data set where data observed during periods of PCA and SWF, and data outside the auroral oval boundaries defined by Starkov (1994) have been removed.

Distributions of HR are shown in Figure 4b and Figure 4e. Similar to Kp, the HR histogram plot is consistent with a log-normal distribution peaking at LOG_{10}(HR)=1.65 LOG_{10}(nT), corresponding to 44 nT, and falling off rapidly with both increasing and decreasing HR. This is also consistent with similar HR distributions presented in Danskin and Lotz (2015). Figure 4e shows that filtering the data set causes a dramatic reduction in the distribution of points for LOG_{10}(HR)<1.6 LOG_{10}(nT) (HR < 40 nT), and an enhancement of the distribution for HR > 40 nT. Geomagnetic activity, and therefore HR, are expected to be enhanced in the auroral region (e.g., Danskin and Lotz, 2015), resulting in the loss of data for low HR, and a shift in the distribution for larger HR. The gap between distributions is largest from 2.0-3.0 LOG_{10}(nT) (100-1000 nT). As HR increases above 1000 nT, the overall data set is dominated by auroral data, and the distributions begin to converge. This shift in HR after filtering is strongly observed for the MEA and SNK station, and to a somewhat lesser extent for FCC and then YKC. Distributions for BLC and IQA (not shown) show very little difference between pre- and post-filtered data. The MEA, SNK, and FCC stations are located at the lowest latitudes and are therefore more likely than the other stations to be located in the sub-auroral region where HR < 100 nT are more common.

Interestingly the highest HR are removed through filtering based on the auroral oval boundaries defined by Starkov (1994), suggesting that magnetic activity is more widespread than the defined auroral oval boundaries suggest. Some of the discrepancy can be attributed to the characterization of the auroral oval by Kp, which varies more slowly than geomagnetic activity and the actual auroral oval boundary.

Figure 4c and Figure 4f show the distributions for LOG_{10}(HRA). Similar to HR and Kp, the distribution for HRA is also log-normal. Note that there is a slight skew to the distribution due to the filtering of data <0.1 dB. The distribution peaks at LOG_{10}(HRA)=-0.4 LOG_{10}(dB) or ~0.4 dB. Unlike HR and Kp, there is very little difference between the filtered and unfiltered data set. Some >5 dB (>0.7 LOG_{10}(dB)) HRA are removed with filtering; these points are associated with PCA. However, several >5 dB intervals remain which can be attributed to auroral absorption.

3.3 Comparison of HRA and Kp

Auroral absorption models typically characterize level of absorption by Kp. Figure 5 shows the relationship between LOG_{10}(HRA) and Kp for each riometer station, and for the entire data set. A logarithmic relationship was evaluated due to the logarithmic nature of Kp (see Section 2.3). An occurrence frequency plot is used where data are binned by 1/3 Kp and 0.05 LOG_{10}(dB), and the number of points within each bin is indicated by color corresponding to the color bar to the right of the plot. Occurrences of zero are not plotted. Due to its high-latitude location, data for the CBB station are only available for Kp<2. For larger Kp the auroral oval shifts to lower latitudes, excluding CBB. Conversely, data for the YKC, FCC, SNK, and MEA stations are only available for Kp>1, 2, 4, and 4+, respectively, due to lower-latitude locations of the stations. As Kp drops below these thresholds the auroral oval contracts such that the equatorward edge is poleward of these stations. Only the BLC and IQA stations are entirely within the auroral boundaries.

Focusing on the BLC, IQA, YKC, FCC, and SNK stations, there is a dense distribution of data, primarily between Kp ≥1 and Kp≤4. This distribution is elongated along a straight line. Overall correlation between LOG_{10}(HRA) and Kp is relatively poor with R<0.50 due to the spread in the data. For Kp<1, the lack of correlation between LOG_{10}(HRA) and Kp suggests that auroral absorption is not regularly observed for such low levels of geomagnetic activity, which is to be expected.

Reduced agreement for Kp>4 can be largely attributed to an overall reduction in the data set for Kp>4. Approximately 87% of the data are weighted to periods of Kp≤4. The limited occurrence of Kp>4 is due to the low geomagnetic activity levels associated with the 2015-2017 period considered here during which time collocated riometer and magnetometer measurements are available compared to previous solar cycles. The 2001-2003 period considered for the FCC data set helped to bolster these statistics as the interval was of higher overall geomagnetic activity. Unfortunately, many of these periods of high geomagnetic activity had to be removed from the data set as they occurred during periods of PCA and absorption could not be entirely attributed to auroral absorption. Uncontaminated Kp>7 data were available over limited periods: 20 March 2001; 1-2,4 October 2002; 18 August 2003; 14 October 2003; 20 November 2003; 17 March 2015; 22-23 June 2015; 7 October 2015.

Black filled circles and vertical lines indicate the average and standard deviation of LOG_{10} (HRA) in bins of 1/3 K_p. Correlation improves significantly for all stations to R>0.85 when considering the binned data. As with the overall distribution, these points follow a relatively straight line until Kp>4, where the data appears to plateau. This plateau is visible in the BLC, IQA, YKC, FCC, and, to a lesser extend, the SNK

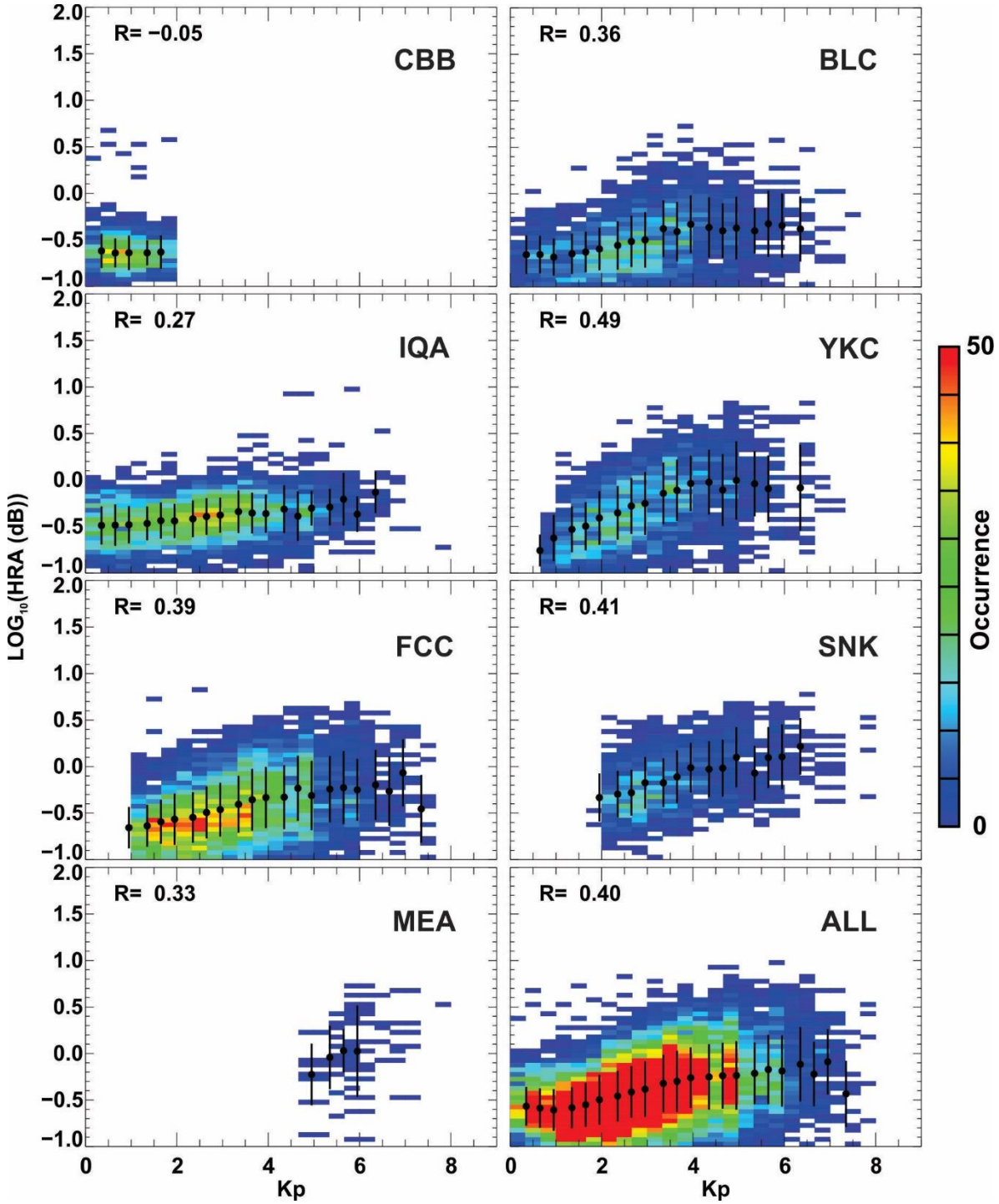

Figure 5: Occurrence density of LOG_{10} (HRA) versus Kp for the filtered data for BLC, CBB, IQA, MEA, SNK, and YKC for 2015-2017, and FCC for 2001-2003, and for the entire data set (ALL). Correlation coefficient (R) is indicated for all data in the plot. Black filled circles and vertical lines indicate the mean and standard deviation of LOG_{10} (HRA) in bins of 1/3 Kp. Mean values are only plotted if at least 10 points were observed in the bin. The maximum occurrence represented by the colour bar is 50 for the station plots, and 100 for the combined data set (ALL).

338 data sets. The standard deviation of data averages is greater for Kp>4 than for Kp<4. Figure 6 shows a
339 comparison between binned data sets in Figure 5. Plateauing for Kp>4 is very clear. The CBB, BLC, IQA,

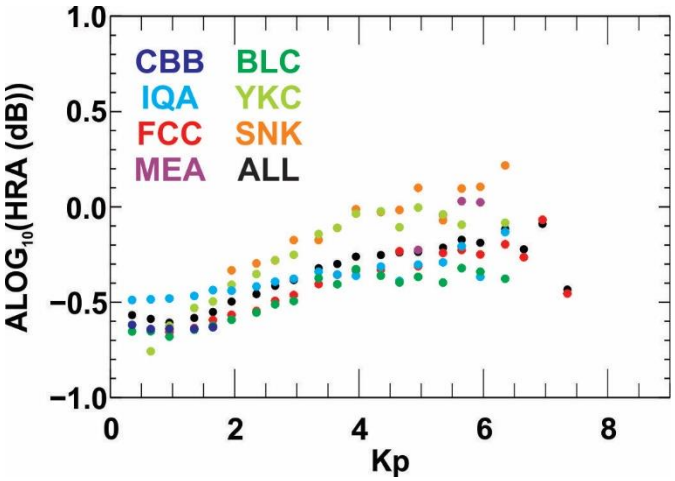

Figure 6: Binned data plotted in Figure 5 for each riometer station and for the overall data set.

FCC, and MEA data sets closely overlap. Importantly, the FCC data, which was derived from a different riometer network, during a different solar cycle, is consistent with NRCan data for 2015-2017. Data for the SNK and YKC stations show slightly higher values of LOG_{10}(HRA) than is observed at other stations. Although SNK and YKC are separated by ~35° longitude, they are located at similar magnetic latitudes in the central auroral oval, which could cause the deviation. FCC has a similar latitudinal location, but is part of a different array and period of observation, explaining the inconsistency with SNK and YKC. Both YKC and SNK have a lower overall occurrence rate than the other stations, which could also contribute to the difference.

Although Figure 5 and Figure 6 represent a reasonable relationship between LOG_{10} (HRA) and Kp, the spread in the data, demonstrated in Figure 5 cannot be ignored, particularly for >1 dB absorption. Based on the plot for all data, the probability of observing >1 dB absorption is roughly equivalent at Kp=1 and Kp=6; the likelihood of observing A=3 dB roughly the same for Kp=2 to 5+.

The relationship between Kp and HRA was further analyzed by considering conditional distributions in terms of both Kp and HRA. Figure 7a shows the normalized distribution of LOG_{10} (HRA) separately for Kp=0, 1, …., 7. Distributions for Kp=8 and Kp=9 are not included due to the lack of data. For Kp ≤ 2 the distributions have identical peaks and very similar spreads. As Kp increases above 4, there is a slight shift in the distribution peak and in the maximum boundary of the distribution, but there is still a large density of data for low HRA. Figure 7b shows the normalized distribution of Kp for different levels of LOG_{10} (HRA). In this distribution there is a clear shift in the peak of the distribution with increasing LOG_{10} (HRA) shifting from Kp=1 in the lowest distribution to Kp=4 in the highest distribution. These distributions further demonstrate that larger Kp correspond to larger LOG_{10} (HRA).

Kavanagh et al. (2004) also examine the relationship between Kp and absorption, and infer a quadratic empirical relationship between parameters, with an MLT dependence on the observed fit. Rather than quantifying the exact nature of the relationship, we instead compare the relationship between Kp and HRA to that of HR and HRA.

3.5 Comparison of HRA and HR

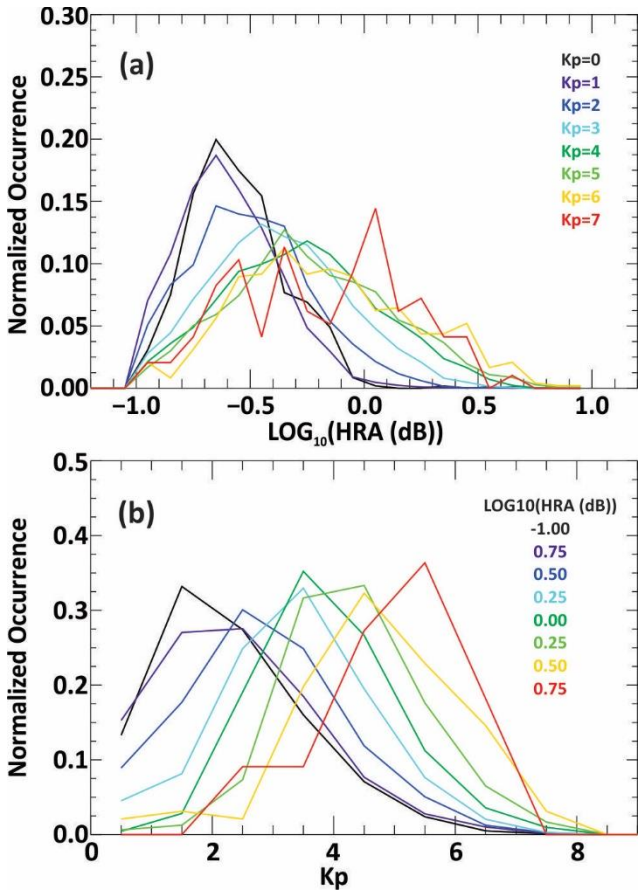

Figure 7: (a) Conditional distribution of LOG_{10} (HRA (dB)) for incremental values of Kp. (b) Conditional distribution of Kp for incremental values of LOG_{10} (HRA (dB)).

Figure 8 shows the relationship between HRA and HR in the same format used in Figure 5. For consistency with Kp index, Figure 8 data are plotted logarithmically. Figure 8 shows occurrence density plot based on data for each station independently, and for all stations together (ALL). Data in the occurrence plots are binned by 0.1 LOG_{10}(nT) in LOG_{10}(HR) and 0.05 LOG_{10}(dB) in LOG_{10}(HRA). For HR<~50 nT (LOG_{10}(HR (nT))~1.7), there is no correlation between HRA and HR; HRA varies between 0.1 dB and 1.0 dB with no indication of a dependency. Auroral absorption is not regularly observed for such periods of low geomagnetic activity, and there is very little data to support a relationship. This lack of relationship is best illustrated for CBB, which is only located within the auroral oval on the dayside and therefore does not typically observe auroral absorption. As HR increases above 50 nT, a clear linear dependence between HR and HRA evolves (R=0.63 for ALL) which is maintained as HR reaches a maximum value of ~2300 nT.

Relationships observed between HR and HRA are more pronounced when considering the average and standard deviation of LOG_{10} (HRA) in bins of LOG_{10} (0.1 nT) for LOG_{10} (HR) (black filled circles and vertical lines in Figure 8). These data are overplotted in Figure 9. Data for each individual station follow very similar trends. As in Figure 6, data for YKC and SNK are slightly elevated compared to the overall data set, although the difference is much less pronounced. Notably, the IQA data are also elevated between LOG_{10} (HR)=[1,2]; IQA riometer data can be noisy and contaminated with spikes. Although efforts were taken to adequately filter the data, this could have resulted in some inconsistently high HRA values and

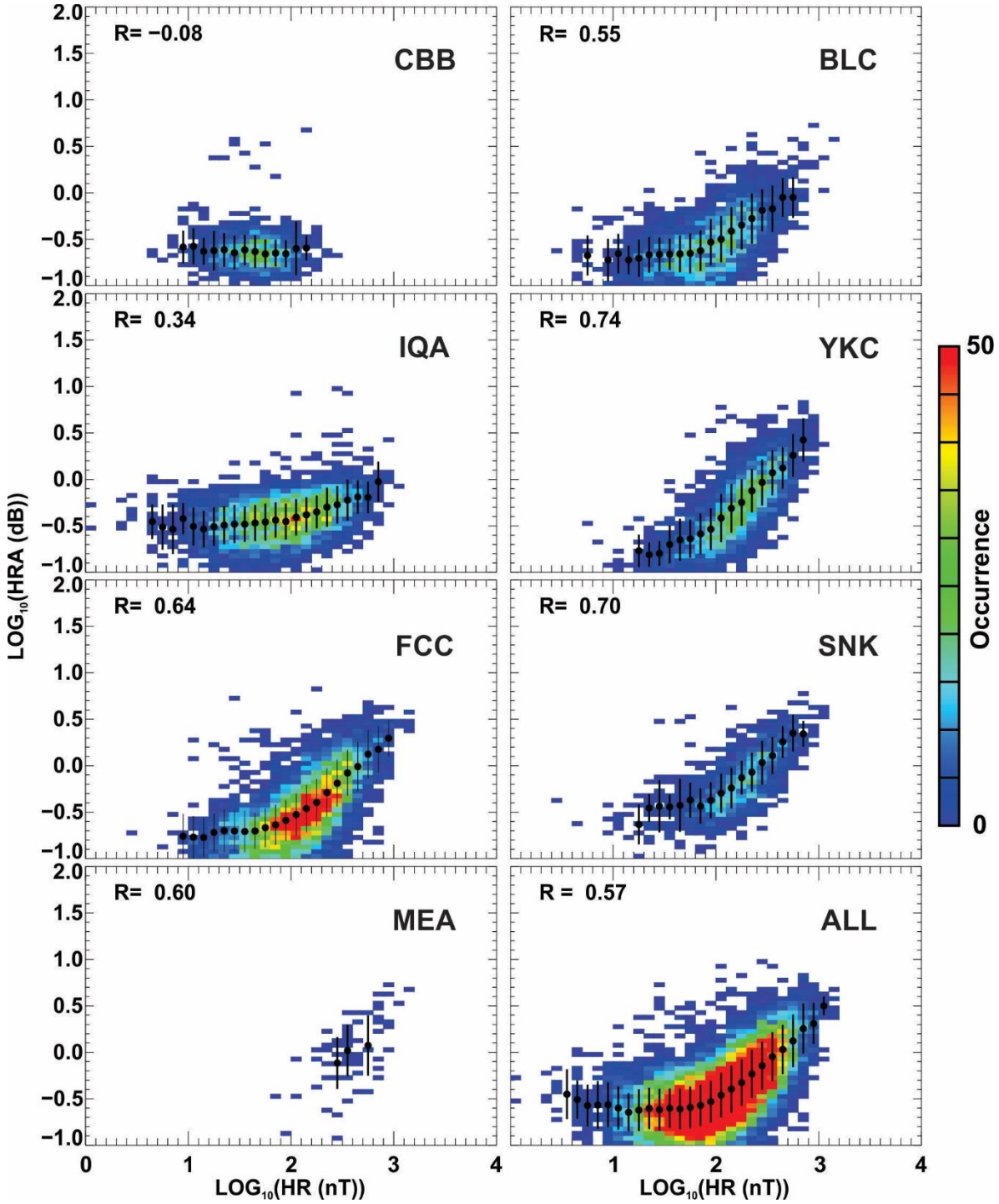

Figure 8: (a) Same as Figure 5 but for LOG_{10}(HRA) and LOG_{10}(HR).

384 may account for some of the discrepancy. Higher HRA at IQA was also demonstrated in Figure 5 for
385 Kp<2 where auroral activity is less likely and noise contamination would therefore standout over auroral
386 absorption, explaining why IQA shows better agreement with other stations for Kp>2.

387 Based on descriptions on the Canadian Space Weather Forecast Center short term magnetic review and
388 forecast website (https://spaceweather.gc.ca/forecast-prevision/short-court/sfst-fr.php), HR values of <

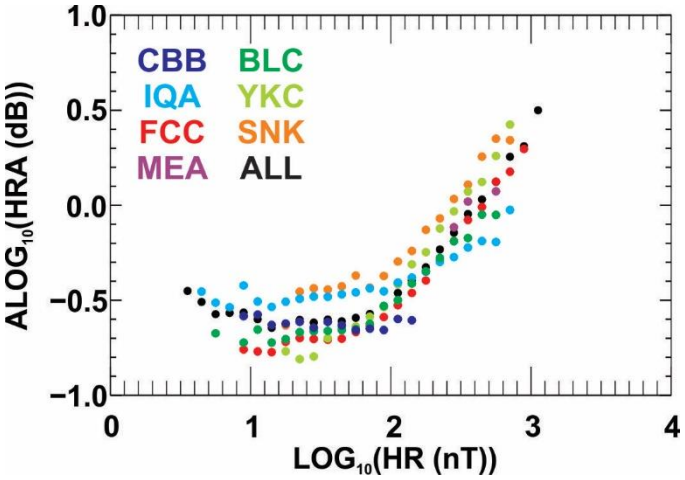

Figure 9: Binned data plotted in Figure 8 for each riometer station and for the overall data set.

50 nT correspond to 'quiet' or low levels of geomagnetic activity, which is the most frequently observed geomagnetic activity level observed in all zones (polar cap, auroral, and sub-auroral) (Danskin et al., 2015). The spread in absorption data is not surprising as there is little 'additional' electron precipitation during quiet geomagnetic conditions. As geomagnetic activity levels increase to more active conditions the HRA changes due to auroral absorption, explaining the change in dependency seen in Figure 8.

Importantly, the distribution illustrated in Figure 8 does not show the same spread in absorption that was observed in Figure 5: 96% of data for HRA > 1 dB corresponds to periods of HR > 50 nT.

4.0 Discussion

Figure 5 and Figure 8 demonstrate the relationships between HRA and Kp and HRA and HR, respectively. Although there appears to be an overall trend of increasing HRA with increasing Kp for Kp≤4, a relationship beyond Kp=4 is not clear due to a plateauing in the data, possible caused by a lack of statistics for large Kp. Regardless, the considerable spread in the data demonstrates that Kp is not a strong parameter for characterizing auroral absorption. HR showed a more promising relationship with HRA. As geomagnetic activity reached active conditions (> 50 nT) at auroral latitudes, LOG_{10} (HRA) was shown to increase linearly with LOG_{10} (HR). Notably, the spread in the data set was considerably reduced from that found between LOG_{10} (HRA) and Kp.

Auroral absorption is a highly dynamic phenomenon responding to energetic electron precipitation in the auroral zone, and is associated with increased geomagnetic activity. As discussed in Section 1, auroral absorption models typically characterize absorption based on global magnetic indices such as the Kp, Ap, or PC indices, or solar wind parameters. We argue that characterization based on a global magnetic index is limiting as auroral absorption is highly variable in time and location.

Figure 10 shows the distribution of HRA and HR in terms of MLT for data from the BLC, FCC, IQA, SNK, and YKC stations. Data in the <09 and >16 MLT sector is attributed to the BLC, FCC, IQA, SNK, and YKC stations. BLC and IQA contribute to both the 09-10 MLT and 15-16 MLT regions. BLC was the only station with observations across the entire MLT sector. CBB observations, which are not included in Figure 10, are limited to the dayside between 10 and 15 MLT and are primarily limited to only low magnitude HR (<200 nT) and HRA (<0.5 dB). Occurrence for MEA was very low and confined to 0-1 MLT and 22-24 MLT, but spanned a wide range of HR (up to ~1000 nT) and HRA (up to ~5 dB). MLT

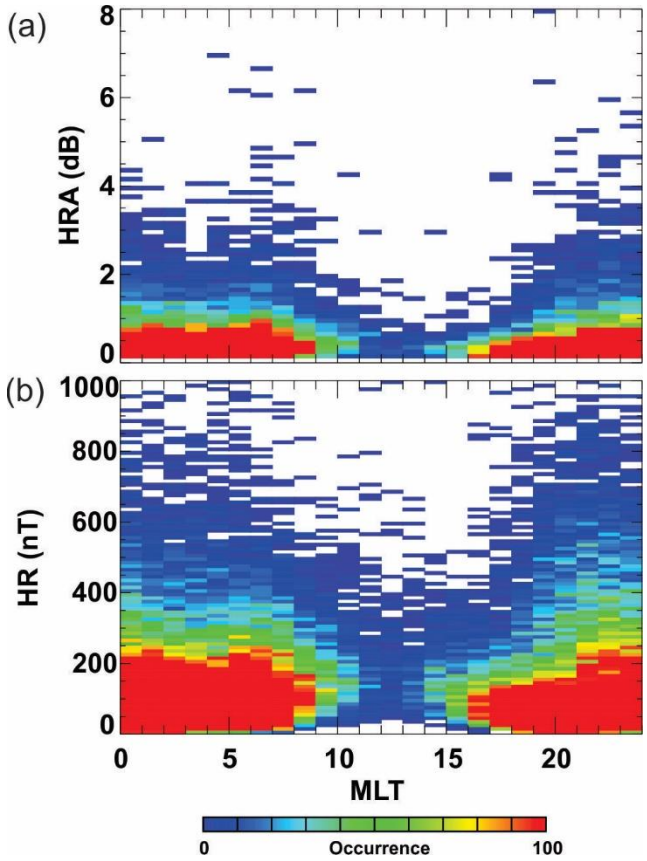

Figure 10: Occurrence distribution of (a) HRA, and (b) HR in terms of MLT using the filtered data set. Data are binned in increments of 1 MLT, 0.1 dB, and 10 nT.

distributions were very similar from station to station (not shown) having (1) higher occurrence across the nightside and low occurrence on the dayside, and (2) a suppression of high HR and HRA on the dayside.

The occurrence of notable HRA > 1 dB (Figure 10a) is most pronounced on the nightside (<9 MLT; >20 MLT) with a notable reduction on the dayside between 10 and 18 MLT, consistent with known distributions of auroral absorption (Basler, 1963; Driatsky, 1966; Frank-Kamenetsky and Troshichev, 2012; Hargreaves 1969; Hartz et al., 1963; Hook, 1968). This Figure illustrates that HRA is not a global phenomenon, as suggested by a global index such as Kp. HR is a better characterization of HRA as it varies on a more local scale. Consider Figure 10b which plots the distribution of HR with MLT. HR is enhanced across the entire nightside, overlapping with both the pre-noon and pre-midnight absorption peaks. MLT variation during periods of heightened geomagnetic activity, as represented by HR, complement the variation observed in HRA. Differences between the HR and HRA distributions indicate that some variations in HR can be caused by processes that do not lead to auroral absorption, which explains some of the spread observed in Figure 8.

The historical choice of using Kp to indicate the level of auroral absorption is not surprising given the availability and reliability of the data. As Menvielle and Berthelier (1991) point out, the Kp index is often used out of 'force of habit'. Unfortunately, the convenience and large-scale use of the Kp index makes it very easy to forget its purpose and meaning. Menvielle and Berthelier (1991) provide a thorough and thought provoking description of the Kp index and include a discussion on the importance

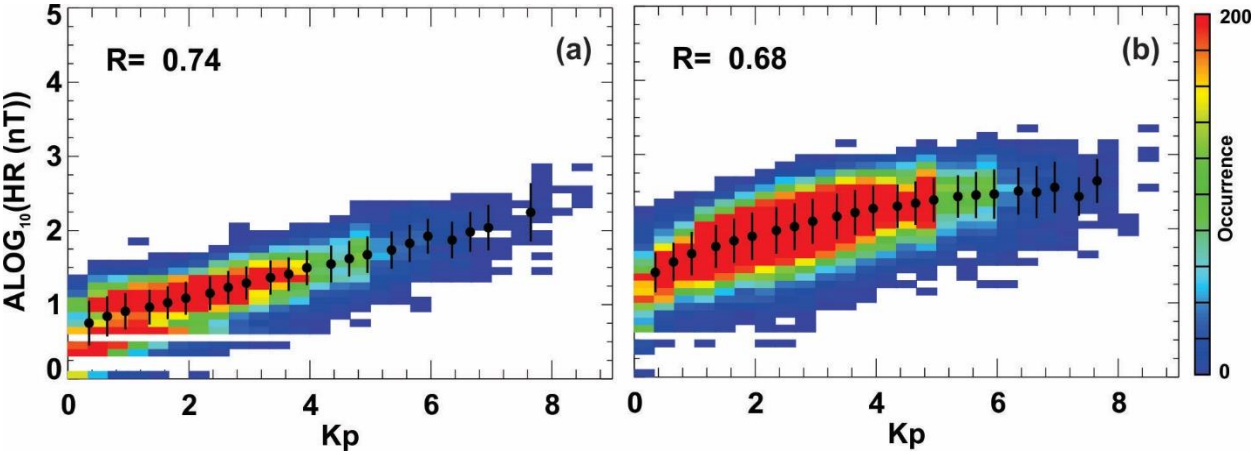

Figure 11: Same as Figure 5 but for LOG_{10} (HR) and Kp. Data in (a) is for the OTT station for 2015-2017 filtered for PCA and SWF, but not for auroral boundaries. Data in (b) is the for same data set processed in Figure 5 and Figure 8.

of using the right index to describe a given phenomenon. The ionospheric / magnetospheric current source of magnetic perturbations varies, depending on the magnetic latitude of the observing station. In the high-latitude polar cap magnetic activity is dominated by reconnection and merging processes on the front-side magnetosphere and magnetotail regions causing the transport of open magnetic field lines over the polar cap. In the auroral region focused on in this paper, magnetic activity is driven by changes in the auroral electrojets and field-aligned currents largely caused by substorm-induced energetic electron precipitation, which also drives auroral absorption. Sub-auroral geomagnetic variations are caused by additional contributions from the ring current, which drives geomagnetic perturbations at equatorial latitudes. Menvielle and Berthelier (1991) point out that the sub-auroral location of the magnetic observatories used to derive the Kp index means that Kp is a good global characterization of magnetic activity because this region is impacted by high, mid, and low-latitude phenomenon. However, this also implies that the Kp index is too broad an index to use to describe a local auroral phenomenon. Substorm-associated activity does not necessarily propagate to low enough latitudes and has a duration that is often less than 3-hours. Menvielle and Berthelier (1991) repeatedly emphasize that Kp index is a mid-latitude (typically sub-auroral) based index intended to characterize global or sub-auroral phenomenon and is not limited to the effect of auroral zone dynamics.

To demonstrate the role of Kp as a sub-auroral, opposed to auroral, descriptor, consider that in the sub-auroral region, there is excellent agreement between Kp and HR. Figure 11a demonstrates this relationship for the Ottawa (OTT) magnetic observatory data for 2015-2017. The occurrence distribution demonstrates a linear trend of increasing LOG_{10}(HR) with increasing Kp. The correlation coefficient is R=0.74, and strongly indicating a linear fit between data sets. Correlation for the binned data is ideal at R=1.00. The observed agreement is not surprising given that Kp is a sub-auroral index to which the OTT magnetometer contributes.

At auroral latitudes geomagnetic activity, and therefore HR, is largely driven by the precipitation of energetic electrons which give rise to the aurora and are typically not observed in the sub-auroral region. Figure 11b plots the logarithm of HR and Kp in the same format used in Figure 11a, and includes data for all stations, similar to Figure 5 and Figure 8. Although correlation is still good at R=0.68, a linear relationship between LOG_{10}(HR) and Kp is not as clear; there is a curve in the distribution that plateaus for Kp≥4. It is possible that some of the plateauing could be attributed to the reduction in data for Kp≥4

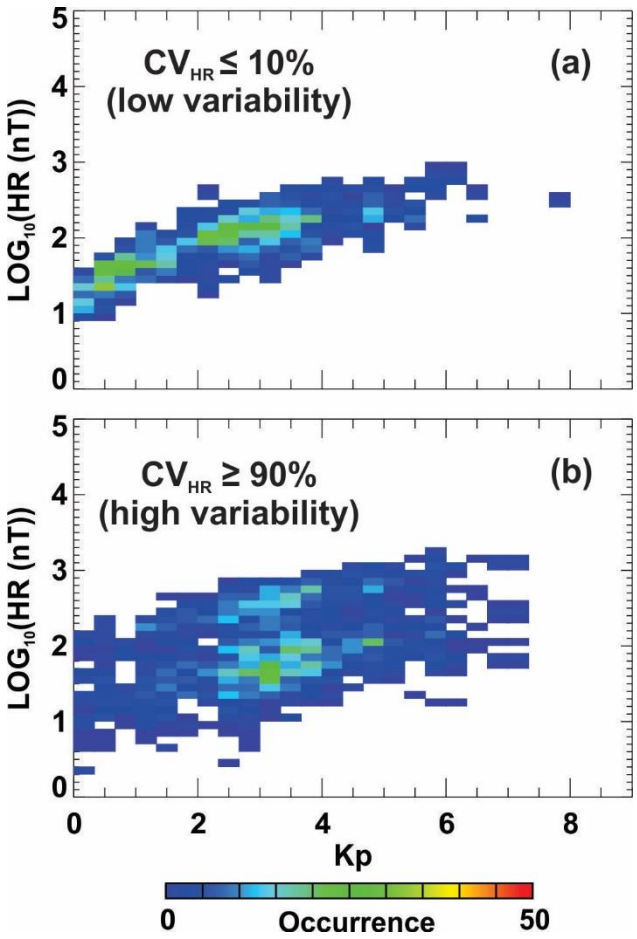

Figure 12: Same as Figure 11b for the subset of points where the coefficient of variation (CV) was (a) <10% and (b) >90%.

(see Figure 4a and 4d). Visually, the lower boundary of the occurrence distribution is linear, whereas the upper boundary begins to plateau for Kp>2. The plateau is associated with a high degree of variation in Kp for a given range of LOG_{10}(HR). For example for LOG_{10}(HR) of ~2.5 Kp varies from 1 to 8.

The degraded relationship between Kp and HR in Figure 11b can be explained by the relationship between the response of HR at auroral and sub-auroral latitudes. Auroral magnetic measurements are sensitive to changes in the auroral electrojet which are not always seen at sub-auroral latitudes, and therefore does not contribute to Kp. If instead the comparison performed is limited to the OTT station, which contributes to Kp, and sub-auroral data are considered, the agreement between Kp and HR is clear, and the plateauing for Kp>3-4 is eliminated.

Kavanagh et al. (2004) points out that Kp is a 3-hour index not capable of capturing the dynamic variation demonstrated for auroral absorption; a statement which motivated a comparison against the more variable HR index. We investigate the variability of the HR index with respect to the Kp index and the role of that variation on the agreement between the Kp index and HRA or HR. To characterize the variability of HR during the 3-hour interval represented by Kp, the coefficient of variation (CV), or relative standard deviation was used. CV is defined as the ratio of the standard deviation of the data divided by the mean. For each 3-hour interval in 2001-2003 (FCC) and 2015-2017 (BLC, CBB, IQA, MEA, SNK, YKC) the coefficient of variation (CV) (or relative standard deviation) in HR was determined (CV_{HR}).

Comparisons between HR and Kp (Figure 11) were evaluated for periods of low variability ($CV_{HR} \leq 10\%$) and periods of high variability ($CV_{HR} \geq 90\%$). Figure 12a and Figure 12b show the low and high variability data for the HR versus Kp comparison, respectively. Low variability data shown in Figure 12b represents 4.6% of the overall data set. Data are weighted to lower-Kp periods (Kp <4), and the data have a high degree of correlation (R=0.81). High variability data, shown in Figure 12d, represents 5.2% of the overall data set. The correlation coefficient is much lower at R=0.46, and there is significant spread in the occurrence plot. Both the low and high variability data show the same plateau for Kp>4, but the data spread is considerably reduced for the low variability subset of data.

The low variability subset of data represent periods where geomagnetic activity is relatively stable across the 3-hour interval represented by the Kp index, whereas the high variability subset of data represent cases where geomagnetic activity significantly increases or decreases between 1-hour periods within the 3-hour interval either at the onset or end of an event, or due to short bursts of active geomagnetic conditions. Agreement between HRA and Kp is affected by the degree of variability represented by CV_{HR} demonstrating the importance of stable conditions for representing HRA by Kp. Such requirements are not needed when characterizing HRA in terms of HR further demonstrating that HR is a more dynamic representation of HRA.

5. Conclusions

The hourly range of absorption (HRA) measured by 7 riometers located in the Canadian auroral region were compared to the Kp index and to the hourly range of the horizontal magnetic field (HR) observed at co-located magnetometers for 2001-2003 (FCC station) and 2015-2017 (BLC, CBB, IQA, MEA, SNK, YKC stations). The following was observed:

1. Distributions of Kp and HR are log-normal, consistent with observations cited in the literature. HRA was also shown to have a log-normal distribution.
2. There is a general linear relationship between LOG_{10}(HRA) and Kp for Kp=[1,4]. For more active geomagnetic conditions (Kp>4), the relationship plateaus and there is large variability such that a range of Kp values are possible, with similar occurrence, for constant LOG_{10}(HRA).
3. Deterioration of the agreement between LOG_{10}(HRA) and Kp for Kp>4 is attributed to (1) the sub-auroral nature of the Kp index compared to the auroral location of energetic electron precipitation causing auroral absorption, (2) the high degree of variability of the geomagnetic field during the 3-hour interval characterized by Kp, and (3) low statistics for large Kp.
4. There is a strong linear agreement between LOG_{10}(HRA) and LOG_{10}(HR) for HR > 50 nT characterized by R=0.63. Variability is considerably reduced compared to Kp; 96% of data for HRA > 1 dB corresponds to periods of HR > 50 nT.

The Kp index is a useful parameter for characterizing global magnetic activity; it is robust and reliable, providing a continuous unbroken data set. However, due to its 3-hour resolution, sub-auroral dependence, and non-sensitivity to auroral disturbances, it is not ideal for characterizing a highly dynamic auroral phenomenon such as auroral absorption, which varies on a local scale at a rate that is frequently <3 hours. HR is a more dynamic characterization of geomagnetic activity varying with a 1-hour resolution based on local geomagnetic activity. As such, it is a more accurate characterization of the level of auroral absorption. Although Kp and solar wind parameters are typically used for auroral absorption modelling, it is recommended that models be developed based on the hourly range of the

magnetic field to obtain a more accurate representation of the local auroral absorption opposed to the general global state.

Acknowledgements

This work was supported by the Natural Resources Canada (NRCan), Lands and Minerals Sector and Public Safety Geosciences program. NRCan magnetic field hourly range data are available online for 2015-2017 (https://www.spaceweather.gc.ca/data-donnee/indices/si-en.php) and from Fiori (2020a) for 2001-2003. NRCan riometer data is available from Fiori (2020b) for the BLC, CBB, IQA, MEA, SNK, and YKC stations for 2015-2017. Data for the FCC riometer for 2001-2003 can be found in the historical Churchill riometer data archive (https://www.ucalgary.ca/aurora/projects/rio), which is maintained by the University of Calgary under support from the Canadian Space Agency. Kp data used in this study were obtained from the National Geophysical Data Centre (ftp://ftp.ngdc.noaa.gov/STP/GEOMAGNETIC_DATA/INDICES/KP_AP/). This is NRCan publication number ##########.

References

Agy, V. (1970), HF radar and auroral absorption, Radio Science 5(11), pp. 1317-1324, https://doi.org/10.1029/RS005i011p01317.

Baker, D. N., P. Stauning, E. W. Hones Jr., P. R. Higbie, and R. D. Belian (1981), Near-equatorial, high-resolution measurements of electron precipitation at L≈6.6, J. Geophys. Res., 86(A4), pp. 2295-2313, https://doi.org/10.1029/JA086iA04p02295.

Basler, R. P. (1963), Radio wave absorption in the auroral ionosphere, J. Geopys. Res., 68 (16), pp. 4665-4681, https://doi.org/10.1029/JZ068i016p04665.

Cannon, P., Angling, M., Barclay, L., Curry, C., Dyer, C., Edwards, R., Greene, G., Hapgood, M., Horne, R., Jackson, D., Mitchell, C., Owen, J., Richards, A., Rogers, C., Ryden, K., Saunders, S., Sweeting, M., Tanner, R., Thomson, A., & Underwood, C. (2013), Extreme space weather: impacts on engineered systems and infrastructure. London, Royal Academy of Engineering

Chisham, G., et al. (2007), A decade of the Super Dual Auroral Radar Network (SuperDARN): scientific achievements, new techniques and future directions, Surveys in Geophysics, 28 (1), 33–109, https://doi.org/10.1007/s10712-007-9017-8.

Coyne., V. J. (Ed.)(1979), Special topics in HF propagation, AGARD Conf. Proc. No. 263, Advisory Group for Aerospace Research and Development, North Atlantic Treaty Organization

Danskin, D. W., Boteler, D., Donovan, E., & Spanswick, E. (2008), The Canadian riometer array, Proc. of the 12th International Ionospheric Effects Symposium, IES 2008

Danskin, D. W., and S. I. Lotz (2015), Analysis of geomagnetic hourly ranges, Space Weather, 13(8), pp. 458-468, https://doi.org/10.1002/2015SW001184.

Desai, M., and J. Giacalone (2016), Large gradual solar energetic particle events, Living Rev. Sol. Phys., 13:3, https://doi.org/10.1007/s41116-016-0002-5.

Driatsky, V. M. (1966), Study of the space and time distribution of auroral absorption according to observations of the riometer network in the Arctic, Geomagnetism and Aeronomy, 6, pp. 828.

Fiori, R.A.D., Nikolic, L., Lam, H.-L., Trichtchenko, L., Danskin, D., McKee, L., Boteler, D. H., Blais, C. (2016), Space Weather Bulletin – 2015; Geological Survey of Canada, Open File 8011, 409 p. https://doi.org/10.4095/297902.

Fiori, R. A. D., D. W. Danskin (2016), Examination of the relationship between riometer-derived absorption and the integral proton flux in the context of modeling polar cap absorption, Space Weather, 14, 1032-1052, https://doi.org/10.1002/2016SW001461.

Fiori, Robyn (2020a), Hourly Range data for: Characterizing auroral absorption based on geomagnetic hourly range, https://doi.org/10.7910/DVN/PKJUFN, Harvard Dataverse, DRAFT VERSION.

Fiori, Robyn (2020b), Riometer data for: Characterizing auroral absorption based on geomagentic hourly range, https://doi.org/10.7910/DVN/V1RJPF, Harvard Dataverse, DRAFT VERSION.

Foppiano, A. J., and P. A. Bradley (1983), Prediction of auroral absorption of high-frequency waves at oblique incidence, Telecommunication Journal, 50(10), pp. 547-560.

Foppiano, A. J., and P. A. Bradley (1984), Day-to-day variability of riometer absorption, J. Atmos. Terr. Phys., 46 (8), pp. 689-696, https://doi.org/10.1016/0021-9169(84)90130-2.

Frank-Kamenetsky, A., and O. Troshichev (2012), A relationship between the auroral absorption and the magnetic activity in the polar cap, J. Atmos. Sol-Terr Physics, 77, 40-45, https://doi.org/10.1016/j.jastp.2011.11.007.

Frissell, N. A., J. S. Vega, E. Markowitz, A. J. Gerrard, W. D. Engelke, P. J. Erickson, E. S. Miller, R. C. Luetzelschwab, J. Bortnik (2019), High-frequency communications response to solar activity in September 2017 as observed by amateur radio networks, Space Weather, 17(1), pp 118-132, https://doi.org/10.1029/2018SW002008.

Hargreaves, J. K. (1966), On the variation of auroral radio absorption with geomagnetic activity, Planet. Space Sci., 14, pp. 991-1006.

Hargreaves, J. K., and F. C. Cowley (1967), Studies of auroral radio absorption events at there magnetic latitudes – I occurrence and statistical properties of the events, Planet. Space Sci, 15, pp. 1571-1583, https://doi.org/10.1016/0032-0633(67)90090-6.

Hargreaves, J. K. (1969), Auroral absorption of HF radio waves in the ionosphere: A review of results from the first decade of riometry, Proceedings of the IEEE, 57(8).

Hargreaves, J. K., H. Ranta, A. Ranta, E. Turunen, and T. Turunen (1987), Observations of the polar cap absorption event of February 1984 by the Eiscat incoherent scatter radar, Planet. Space Sci., 35 (7), pp. 947-958.

Hargreaves, J. K. (2007), Seasonal variations in the incidence of auroral radio absorption events at very high latitude, and the influence of the magnetotail, Ann. Geophys., 25, pp. 711-720.

Hargreaves, J. K. (2010), Auroral radio absorption: The prediction question, Adv. Space Res., 45, pp. 1075–1092, https://doi.org/10.1016/j.asr.2009.10.026.

Hartz, T. R., L. E. Montbriand, and E. L. Vogan (1963), A study of auroral absorption at 30 MC/S, Canadian Journal of Physics, 41.

Hartz, T. R., L. E. Montbriand, and E. L. Vogan (1963), A study of auroral absorption at 30 MC/S, Canadian Journal of Physics, 41, pp. 581-595.

Holt, C., B. Landmark, F. Lied (1961) Analysis of riometer observations obtained during polar radio blackouts, J. Atmos. and Terr. Phys., 23, pp. 229-230, https://doi.org/10.1016/0021-9169(61)90048-4.

Hook, J. L. (1968), Morphology of auroral zone radiowave absorption in the Alaska sector, J. Atmos. and Terr. Phys., 30(7), pp. 1341-1351), https://doi.org/10.1016/S0021-9169(68)91192-6.

Hruska, J., and R. L. Coles (1987), A new type of magnetic activity forecast for high geomagnetic latitudes, Journ. of Geomag. and Geoelectr., 39(9), 521-534, https://doi.org/10.5636/jgg.39.521.

ICAO (2018), Annex 3 to the Convention on International Civil Aviation, Meteorological Service for International Air Navigation, ICAO International Standards and Recommended Practices, Twentieth Edition, July 2018, http://store.icao.int/products/annex-3-meteorological-service-for-international-air-navigation (last accessed 11 June 2020).

ICAO (2019), Manual on Space Weather Information in Support of International Air Navigation, ICAO Doc 10100, First Edition, https://store.icao.int/products/manual-on-space-weather-information-in-support-of-international-air-navigation-doc-10100 (last accessed 11 June 2020).

Kavanagh A.J., Kosch M.J., Honary F, Senior A, Marple S.R., Woodfield E.E, and McCrea I.W (2004). The statistical dependence of auroral absorption on geomagnetic and solar wind parameters, Ann. Geophys., volume 22, issue3, pp. 877-887.

Lam, H.-L. (2011), From early exploration to space weather forecasts: Canada's geomagnetic odyssey. *Space Weather*, 9, https://doi.org/10.1029/2011SW000664.

Liang, J., W. W. Liu, E. Spanswick, and E. F. Donovan (2007), Azimuthal structures of substorm electron injection and their signatures in riometer observations, J. Geophys. Res., 112 (A09209), https://doi.org/10.1029/2007JA012354.

Mayaud, P. N., Analyse d'une série centenaire d'indices d'activité magnétique, III, La distribution de fréquence est-elle logarithmonormale?, Ann. Geophys., 32, 443, 1976.

Menvielle, M., and A. Berthelier (1991), The K-derived planetary indices: description and availability, Reviews of Geophysics, 29 (3), pp. 415-432.

Nielsen, E., and F. Honary (2000), Observations of ionospheric flows and particle precipitation following a sudden commencement. Ann. Geophys., 18, 908-917, doi:10.1007/s00585-000-0908-y.

National Research Council (2008), Severe space weather events – Understanding societal and economic impacts: a workshop report, *Natl. Acad. Press*, Washington, D.C., pp 144.

Neal, J. J., Rodger, C. J., & Green, J. C. (2013), Empirical determination of solar proton access to the atmosphere: Impact on polar flight paths, *Space Weather*, 11, 420-4333, https://doi.org/10.1002/swe.20066.

Newell, P. T., R. A. Greenwald, J. M. Ruohoniemi (2001), The role of the ionosphere in aurora and space weather, Reviews of Geophysics, 39(2), pp. 137-149.

NORSTAR (2014). CANOPUS quiet day curve generation. Available online: http://aurora.phys.ucalgary.ca/norstar/rio/doc/CANOPUS_Riometer_Baselining.pdf (accessed 01 March 2019).

Ogunmodimu, O. A. (2016), Auroral radio absorption: Modelling and Prediction, Ph. D. Thesis, Lancaster University.

Pirjola, R., Kauristie, K., Lappalainen, H., Viljanen, A., & Pulkkinen, A. (2005), Space weather risk, *Space Weather*, 3 (S02A02), https://doi.org/10.1029/2004SW000112.

Redmon,R.J., D. B. Seaton, R. Steenburgh, J. He, and J. V. Rodriguez (2018). September 2017's geoeffective space weather and impacts to Caribbean radio communications during hurricane response. Space Weather, 16, 1190–1201. https://doi.org/10.1029/2018SW001897.

Rogers, N. C., and F. Honary (2015), Assimilation of real-time riometer measurements into models of 30 MHz polar cap absorption, Journal of Space Weather and Space Climate, 5, pp. 1-18., https://doi.org/10.1051/swsc/2015009.

Rogers, N. C., A. Kero, F. Honary, P. T. Verronen, and E. M. Warrington (2016a), Improving the twilight model for polar cap absorption nowcasts, Space Weather, 14, 950-972, https://doi.org/10.1002/2016SW001527.

Rostoker, G., Samson, J. C., Creutzberg, F., Hughes, T. J., McDiarmid, D. R., McNamara, A. G., Vallance, A. Jones, Wallis, D. D., & Cogger, L. L. (1995), CANOPUS – A ground-based instrument array for remote sensing the high latitude ionosphere during the ISTP/GGS program, *Space Science Reviews*, 71(1), 743-760, https://doi.org/10.1007/BF00751349.

Sauer, H., and D. C. Wilkinson (2008), Global mapping of ionospheric HF/VHF radio wave absorption due to solar energetic protons, Space Weather, 6, S12002, https://doi.org/10.1029/2008SW000399.

Serson, P. H. (1957), An electrical recording magnetometer, Canadian Journal of Physics, 35(12), 1387-1394, https://doi.org/10.1139/p57-150.

Sigernes, F., M. Dyrland, P. Brekke, S. Chernouss, D. A. Lorentzen, K. Oksavik, and C. S. Deehr (2011), Two methods to forecast auroral displays, J. Space Weather Space Clim, 1 (A03), https://doi.org/10.1051/swsc/2011003.

Spanswick, E., E. Donovan, W. Liu, D. Wallis, A. Aasnes, T. Hiebert, B. Jackel, M. Henderson, H. Frey (2005), Substorm associated spikes in high energy particle precipitation, Geophysical Monograph Series, 155, pp. 227-236, https://doi.org/10.1029/155GM24.

Starkov, G.V. (1994), Mathematical model of the auroral boundaries, Geomag. Aeron., 34 (3), 331–336.

Thayaparan, T., Y. Ibrahim, J. Polak, and R. Riddolls (2018), High-frequency over-the-horizon-radar in Canada, IEEE Trans. Geosci. Remote Sens., 15(11), pp. 1700-1704, https://doi.org/10.1109/LGRS.2018.2856185.

Trichtchenko, L., H.-L. Lam, D. H. Boteler, R. L. Coles, J. Parmelee (2009), Canadian space weather services, Canadian Aeronautics and Space Journal, 55(2), pp. 107-113, https://doi.org/10.5589/q09-013.

Yamagishi, H., Y. Fujita, N. Sato, P. Stauning, M. Nishino, K. Makita (1998), Conjugate features of auroras observed by TV cameras and imaging riometers at auroral zone and polar cap conjugate-pair stations. In: Moen J., Egeland A., Lockwood M. (eds) Polar Cap Boundary Phenomena. NATO ASI Series (Series C: Mathematical and Physical Sciences), vol 509. Springer, Dordrecht.